applied sciences

MDPI

Article

SHS Produced TiB_2-Si Powders for Selective Laser Melting of Ceramic-Based Composite

Le Liu, Sofiya Aydinyan, Tatevik Minasyan and Irina Hussainova *

Department of Industrial and Mechanical Engineering, Tallinn University of Technology, Ehitajate 5, 19180 Tallinn, Estonia; le.liu@taltech.ee (L.L.); sofiya.aydinyan@taltech.ee (S.A.); tatevik.minasyan@taltech.ee (T.M.)

* Correspondence: irina.hussainova@taltech.ee; Tel.: +372-58143868

Received: 9 March 2020; Accepted: 4 May 2020; Published: 8 May 2020

Abstract: One of the main limitations for widespread additive manufacturing is availability and processability of the precursor materials feedstock. For the first time, this study reports the development of a "pomegranate-like" structured TiB_2-Si ceramic-metalloid powder feedstock suitable for selective laser melting (SLM) of ceramic-based composite. The powder was produced via self-propagating high temperature synthesis (SHS) at a moderate combustion temperature of 1530 °C. The effective activation energy in the Ti-B-Si system for the slow step of the combustion process was estimated as 184 kJ. Conditions of SHS process demonstrated a strong influence on the properties of produced powders and, therefore, on SLM parameters and properties of the printed materials. The powders have demonstrated a high performance for manufacturing bulks of 56 wt%TiB_2–44 wt%Si ceramic-based composite.

Keywords: titanium diboride; ceramic composite; selective laser melting; self-propagating high-temperature synthesis

1. Introduction

Recent progress in materials science and technology has established a new paradigm in producing visual models of 3D architectures by additive manufacturing (AM) or 3D printing. AM represents a continuously growing multi-billion-dollar industry and has a profound impact on society and culture [1–3] as this technology allows for the fabrication of precisely dimensioned high-value products with specified internal features without extensive tooling.

The growing interest in the manufacturing of high-performance components for applications in biomedical, aerospace, and automotive industries exemplifies the need for development of high-temperature (HT) ceramic materials with the help of AM [4]. While still at its infancy, direct AM processing of ceramics or ceramic-based composites requires the development of specific precursor materials and procedures to sinter them.

Thorough selection of feedstock powders, which highly affect structures, properties, and performance of final product, is urgently needed for the fabrication of defect-free, structurally sound, and reliable AM parts. An ability to add functionality requires not only the precise control over the process, but also the efficiency of powders used. Production of AM parts with consistent, repeatable, and predictable characteristics depends on input materials. Although a wide variety of available methods offer powerful features and impressive capabilities, one of the key hurdles impeding wider application of AM is the current severe limitation of materials feedstock suitable for direct or indirect AM processing [4,5]. The main advantage of the direct AM route is a simultaneous combination of forming and densification steps, which allows generation of the final component without any post-treatment. The direct selective laser melting (SLM) is one of the most convenient and reliable

methods for producing polymer- and/or metal-matrix composites [3,4]. A relatively wide range of metallic powders has been developed for AM; however, there is a lack of ceramic or ceramic-based powders available for AM through SLM. The process of building defect-free dense ceramic parts by SLM remains challenging due to the extremely high melting point, poor thermal shock resistance, and low or no plasticity of ceramics [5,6]. Commonly, the components fabricated by the direct SLM exhibit a high level of porosity and poor mechanical properties. One of the approaches is combining ceramic particles with a metal/metalloid binder, which ideally represents core-shell structures with a ceramic core responsible for mechanical properties and a metallic shell needed for laser absorptivity and material ductility. Production of custom-made items of a high performance and economic efficiency necessitates the utilization of powdered feedstock, which meets the requirements posed by the AM process conditions [7]. Therefore, the development of powder materials with tailorable physical and chemical properties has attracted a great deal of attention in the research community and industry.

The quality of the feedstock powders largely depends on manufacturing process. The alloy powders are mainly prepared with the help of either the gas atomization process, rotary atomization process, or plasma rotating electrode process (PREP) [8]. The importance of a cost-effective production of powders with controlled particle size distribution and purity is a driving force for the development of several innovative concepts.

We report on the exploitation of the energy-efficient and time-saving method of self-propagating high-temperature synthesis (SHS) or combustion synthesis (CS) [9,10] to design and produce the ceramic-metal powders for AM process [11,12]. We demonstrate the "pomegranate-like" TiB_2-Si powder particulates to be suitable for SLM of the ceramic-based composite of high ceramic fraction.

The main characteristics of the feedstock materials, which govern the powders flowability during the layer building, include shape, size distribution, surface morphology, and composition [8]. Fine particles may undergo a significant aggregation, while large particles reduce the maximum layer packing density. Optimization and precise control of combustion synthesis (e.g., combustion temperature, velocity, cooling rate, etc.) ensure production of the feedstock exhibiting the pre-requisite characteristics.

An increasing demand for properly designed engineering ceramics needed for armor, hypersonic aerospace vehicles, and electronically conductive ceramics has resumed an interest in titanium diboride-based materials due to their high melting point and high temperature stability, remarkable hardness and stiffness combined with a good fracture toughness, and their electrical- and thermal-conductivity [13]. The main limiting factor for wide application of these materials is their poor sinterability related to the exaggerated grain growth and spontaneous mechanical degradation by an internal stress-induced cracking during cooling from a high sintering temperature [13,14]. Another disadvantage is reasoned by the economic factors, particularly the high cost of the consolidation ongoing at temperatures in the range of 1800–2300 °C. One of the approaches to fabricate the materials of high density is a liquid phase sintering with metallic additives, which promotes a fast particle re-arrangement and further densification [15]. The liquid phase sintering, however, also fosters rapid mass transport through the melt and considerably accelerates grain growth. Therefore, to prevent the grain growth, the use of a minimum volume of liquid phase or the implementation of grain growth retarding additives is needed.

The drawbacks in producing and shaping products are the main concerns, which can be solved by a powder-based AM technique such as SLM enabling layer-by-layer fabrication of complex 3D structures. In [16], the fabrication of TiB_2 reinforced Al-matrix composites by the combustion synthesis was reported; however, the printed parts of uncontrolled porosity were obtained. TiB_2 decorated AlSi10Mg composite (NTD-Al) powder was prepared in [17] using a gas-atomization procedure. Ti-TiB (monoboride) cermets were in situ produced from Ti-(5–15 wt%TiB_2) mixtures using SLM, and they demonstrated promising results for future developments [18–20]; however, titanium diboride based ceramics have not yet been produced with the help of AM.

The present work reports a strategy for the preparation of TiB_2-Si powders for AM by the self-propagating high temperature synthesis (SHS). TiB_2-Si bulks were fabricated out of the combustion

synthesized "pomegranate-like" TiB_2-Si precursor powders, which, to the best of our knowledge, are unique and have not been yet documented elsewhere.

Laser melting of a single-component powder (either Si or TiB_2) is a rather complicated process due to a very narrow processing window, especially for ceramics of a high melting point. A tendency of melt surface to shrink and minimize the surface energy results in the formation of re-solidified droplets. Therefore, the high-melting point powders (such as TiB_2) are usually mixed with the relatively low-melting point binding powders (here Si). The addition of silicon to TiB_2 yields to increase fluidity, which reduces cracking during solidification and minimizes shrinkage porosity. The presence of silicon significantly decreases the surface tension and viscosity of the pool. The optical properties of silicon, studied in a broad range of laser wavelength (500–1500 nm) under the atmospheric pressure, demonstrated that an average absorption of a silicon slab (20–260 μm) makes 61%, 41%, and 0.5% at 500 nm, 1000 nm, and 1500 nm of laser wavelength, respectively [21]. Generally, powdered materials exhibit a significantly higher absorptance than their dense form; thus, silicon absorption at 1.07 μm wavelength of Yb-fiber laser is >41%. On the other hand, borides have been shown to be good absorbers in the range of 500–900 nm with the reflectance of about 50%. Based on the estimation of borides absorption given in [22], the absorptance of TiB_2-Si powder mixture can be roughly assessed to be ~45% for materials comprising of 60 vol%Si. Therefore, the composition of 56 wt%TiB_2–44 wt%Si has been chosen for consideration.

2. Materials and Methods

2.1. Self-Propagating High Temperature Synthesis of TiB_2-Si Composite Powder

The commercially pure materials listed in Table 1 were used for the combustion synthesis of the precursor powder. The density of the synthesized powder in its reference state is 1.2 g mL^{-1}. A green mixture of reactants was homogenized in a ceramic mortar for 15 min to prepare the cylindrical samples of 2.1–2.3 g·cm^{-3} density, 30–35 mm height, and 20 mm diameter with the help of uniaxial pressing of 5 kN. Two C-type tungsten-rhenium thermocouples (wire diameter 0.1 mm) covered with a thin layer of boron nitride were positioned in the holes (diameter 1 mm, depth 10 mm) drilled in each sample to record the temperature-time profiles of the combustion process.

Table 1. Precursor powders.

No	Precursor	Particle Size, μm	Producer	Purity, %
1	Ti	20	Alfa Aesar	>99
2	B	<1	amorphous powder (Sigma-Aldrich)	>95
3	Si	20	Sigma-Aldrich	>98

The samples were placed into a reaction chamber CPR-3.5l, which was sealed, evacuated, purged, and filled with argon of 99.999% purity to the pressure of 0.5–2 MPa. To initiate the combustion reaction, a short-term annealing of a tungsten coil (12 V, 1–2 s) positioned on the upper surface of a sample was employed. Maximum combustion temperature (T_c) for each sample was calculated as an average of the maximum for two temperature profiles. The average value of combustion velocity was calculated as $U_c = L{\cdot}t^{-1}$, where L is a distance between the thermocouples, and t is a time between the signals of the thermocouples. The standard error of measurement for T_c and U_c was ±20 °C and 5%, respectively. After the combustion process, TiB_2-Si samples were ground into powder in a laboratory porcelain mortar by pestle and sieved to the fraction of 20–45 μm.

2.2. Selective Laser Melting of TiB_2-Si

The SHS-ed TiB_2-Si powders were printed as solid cylinders (Ø10 × 5 mm) with the help of SLM apparatus (ReaLizer 50 GmbH, Germany) at the conditions listed in Table 2. The SLM machine employs a high powered continuous-wave laser, which is modulated to function like a pulsed laser

system. The Yb:YAG fiber laser with a maximum power of 120 W and wavelength of 1.07 μm was used to solidify the structures under consideration. The process of SLM was performed in the argon atmosphere of high purity (99.999 vol.%) using 1400–2200 mA, at a scanning speed of 80 mm·s^{-1}. Point distance and exposure time were chosen as 10 μm and 125 μs, respectively. As median diameter (D50) of the synthesized TiB_2-Si particles was measured to be 21 μm, the single layer thickness of 25 μm was chosen accordingly. A "zig-zag" scan strategy, in which the laser pattern rotates by 60° after each layer, was used to fabricate the samples.

Table 2. Laser current and volumetric energy density applied to produce TiB_2-Si solid parts.

No.	Laser Current(mA)	Volumetric Energy Density (J·mm^{-3})
Cylinder 1	1400	280
Cylinder 2	1800	360
Cylinder 3	2200	440

2.3. Characterization of Powders and Printed Parts

Standard feedstock characterization techniques for industry are defined in ASTM F3049 (Standard Guide for Characterizing Properties of Metal Powders), which is specified for the powder metallurgy. Nevertheless, these techniques may be used to estimate powders flowability for AM processing. In this work, the flowability was evaluated using the Hall Flowmeter test as a time of 50 g of powder flowing through the Ø2.5 mm hole in a funnel according to the EVS-EN ISO 4490:2018 standard. At least five measurements were carried out and values were averaged. The particle size distribution was assessed with the help of laser diffraction using a Malvern Mastersizer 3000.

The bulk density of the prepared composites was measured by Archimedes' method (Mettler Toledo ME204, Australia) using distilled water as the immersion medium. The theoretical density was estimated assuming a rule of mixture and taking the density of TiB_2 and Si as 4.49 g cm^{-3} and 2.33 g cm^{-3}, respectively. Phases analysis of the samples, which were crashed into powders, was performed by X-ray diffraction (XRD) using a Philips X'Pert PRO diffractometer (40 mA, 40 kV, CuKα radiation, λ = 0.1542 nm, step size of 0.02°, PANalytical, Netherlands) for both powders and as-printed specimens. The XRD peaks were determined from the HighScore Plus software database (ICSD-cross referenced). The relative contents of the phases presented in the structures were estimated by the Rietveld refinement method, which was performed by quantitative analysis of the crystalline phases detected by corresponding XRD patterns (TiB_2-ICDD card No. 04-002-0799 and Si-ICDD card No. 04-014-8844).

For microstructural analysis, a field-emission scanning electron microscope (FE-SEM, Zeiss Evo MA15, Germany) equipped with an EDS (energy dispersive spectroscopy) detector was utilized. Samples were subjected to a hot conductive (resin) mounting, polished with the diamond abrasives down to 0.5 μm finish and coated with a thin layer of Pt for better conductivity.

Micro-hardness measurements were conducted using the Vickers microhardness tester (Indentec 5030 SKV) at a load of 1 kg for a dwell time of 10 s. The measured hardness value for each specimen was taken as the average of 10 indents.

The surface roughness analysis was performed by a Keyence VK-X250 profile-analyzing confocal laser microscope (Keyence Corporation, Osaka, Japan). Maximum height (Sz) and arithmetical mean height (Sa) were averaged for four scanned areas with the dimensions of 500 μm × 700 μm. Sz is a sum of the maximum peak height and the maximum valley depth in the defined area, and Sa is the average value of the absolute height at each point.

3. Results and Discussion

3.1. Combustion Dynthesis in the Ti-B-Si System

The SHS process is a self-sustained combustion where the heat is generated by the direct synthesis reaction to support combustion wave propagation. The combustion synthesis was performed based on thermodynamic calculations taking into consideration a temperature of TiB_2/Si formation (~1430 °C) [15]. The combustion limit was achieved for the mixture with n (Si) = 2.75 regardless to the ambient gas pressure (0.1–2 MPa) and the relative density of the initial specimen (30–60%). Combustion temperature was 100–500 °C lower than the adiabatic temperature, which is conditioned by large heat losses through radiation and the geometrical set-up of the apparatus. According to the thermodynamic model of the Ti-B-Si system, the formation of TiB_2 is a spontaneous process due to negative Gibbs free energy (ΔG^0_T) at the calculated temperature interval (1500–2000 K). At temperatures exceeding 1700 K, the evolution of titanium monoboride (TiB) and titanium silicides (TiSi) may be considered as the competitive processes to TiB_2 formation. Therefore, the combustion synthesis was performed in the Ti-2B-***n***Si system at a temperature around 1700 K to avoid by-products and to provide formation of TiB_2-Si fine particles. An amount of silicon was varied from 1 up to 3 moles to ensure a sufficient quantity of liquid silicon fuse to cover titanium diboride particulates.

Parameters of the combustion process in the Ti-B-***n***Si mixtures are highly affected by the amount of silicon. At a silicon content of n = 2.75 moles, Si occupies ~63 vol.% of the Ti-B-Si mixture. Considering the packing geometry of Ti, B, Si particles, a heat transfer at the Ti-B interface mostly occurs through silicon particles during the combustion reaction.

Low thermal conductivity of boron (0. 26 $W{\cdot}cm^{-1}{\cdot}K^{-1}$ at 300 K) and silicon (1.42 $W{\cdot}cm^{-1}{\cdot}K^{-1}$ at 300 K and 0.287 $W{\cdot}cm^{-1}{\cdot}K^{-1}$ at 1400 K) may result in an inhomogeneous heat transfer and consequent interruption of the CS reaction. Both combustion temperature and velocity decrease with an increase in Si amount in the initial mixture. As illustrated in Figure 1a, a combustion limit is achieved below the melting point of silicon. The combustion wave propagation in the Ti-B-Si system is also governed by the size of the specimen. Pilot batches of 30 × 40 × 120 mm^3 provided a complete conversion of reagents attributed to decreased radial heat losses; therefore, the combustion temperature was equal to the adiabatic temperature.

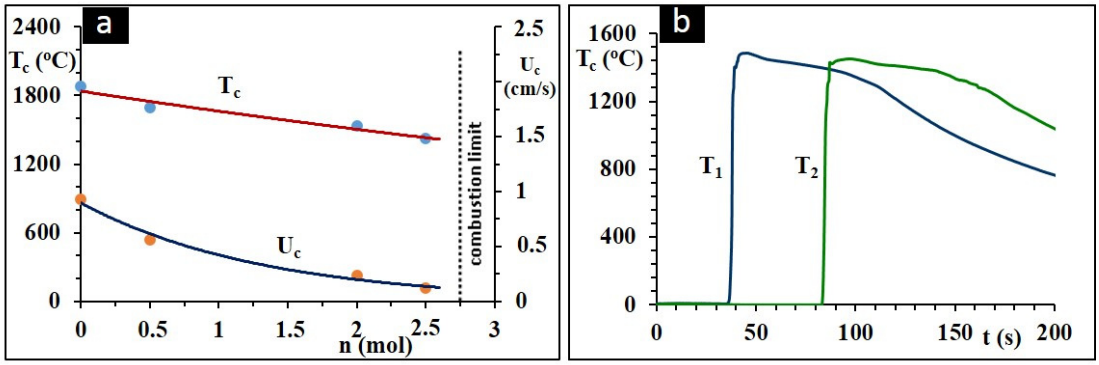

Figure 1. Combustion law for Ti + 2B + ***n***Si system (**a**), and combustion thermograms of Ti + 2B + 2Si mixture (**b**) at $P_{(Argon)}$ = 1 MPa.

At a lower than stoichiometric amount of the boron source, the formation of titanium silicides (TiSi, Ti_5Si_3) and titanium monoboride (TiB) becomes favorable. In terms of preparation of the TiB_2-Si composite powder, where nano- or ultra-fine scaled TiB_2 particles are held together by molten silicon, the stoichiometric amounts of titanium and boron are relevant at the silicon amount of 2 moles at the combustion temperature over the melting point of silicon. The interaction of the solid Ti particles with the melt of Si or eutectics in the combustion wave was reported in the temperature interval 1330 °C < T < 1670 °C [23,24] accompanied by the formation of $TiSi_2$ and TiSi. In these works, it was

shown that the interaction between the reagents at a temperature of 1330 °C, which is below all reactant melting points, occurs through the eutectic reaction, L = $TiSi_2$ + Si (L-liquid). At higher temperatures, the fusion of both silicon and titanium appears to proceed almost simultaneously and results in the formation of Ti_5Si_3. In the system under consideration, the formation of only trace amounts of TiSi was observed in the non-stoichiometric mixtures. At a high temperature, the amount of silicon is deficient for $TiSi_2$ formation, while at a low temperature, the $TiSi_2$ formation is unlikely. At a temperature below the Si melting point (1414 °C), the eutectic reaction (L = Ti + $TiSi_3$) is not detected.

The combustion front progresses from top to bottom of the specimen with an undulating movement in the presence of silicon. This combustion mode differs from the smooth planar wave observed in an undiluted Ti-B. As the combustion temperature is decreased by the silicon diluent, the wave propagation is recorded to be unstable. The undulating movement produces a layered structure in the product as shown in Figure S1. This type of wave propagation is influenced by a liquid phase in the front; thus, the Arrhenius plot of the activation energy for the slow step in the combustion reaction may be determined. The effective activation energy was estimated as 184 kJ assuming no change in the phase composition, Figure S1.

In [25], the effective activation energy of 539 kJ and 318 kJ has been reported for the reaction to form TiB_2 and 410 kJ for the combustion of Ti + 1.5B with the formation of the TiB_2 + TiB mixture. Inferior values of the activation energy suggest a liquid state mechanism rather than the participation of a solid phase in the combustion reaction in the Ti-B-Si system. During the combustion of the Ti + 2B + 2Si mixture, a wave is propagated with a velocity of 0.24 $cm \cdot s^{-1}$ reaching the maximum combustion temperature of 1530 °C, as in Figure 1b. Figure 2 represents the product after the SHS process demonstrating a highly porous bulk, which easily can be powdered by milling. Figure 2b demonstrates the SEM image of the product of Ti + 2B + ***n***Si (n = 1.5–2 moles) mixture after milling, which represents a collection of particles (<50 μm) and their agglomerates (~0.1 mm). The diameters of the chosen particulates, labelled as *Da1, Da2, Da3* in Figure 2c, were estimated to be 436 nm, 349 nm, and 267 nm, respectively, asserting particulates sizes in the 200–450 nm range.

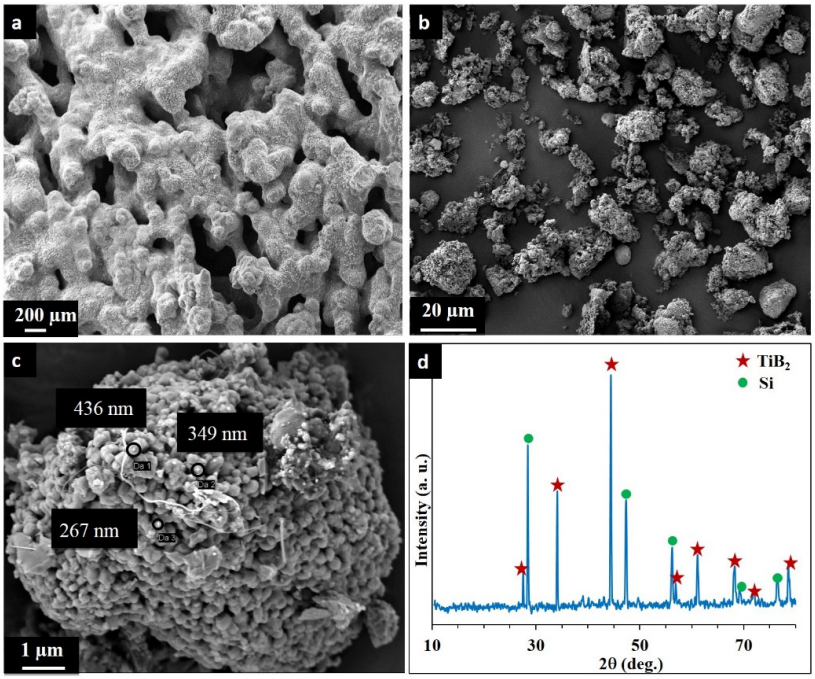

Figure 2. Scanning electron microscope (SEM) images of porous bulk TiB_2-Si product produced by SHS (**a**), the TiB_2-Si powder after milling (**b**,**c**), and the X-ray diffraction (XRD) pattern of the combustion product (**d**).

Morphology of the starting powders defines the degree of particles packing throughout the deposited layer. It is well-documented that spherical particles improve the flowability of powders and, therefore, highly affect the quality of the printed product. The SHS method utilized for the preparation of the TiB_2-Si feedstock allows for the production of irregular-shaped particles with the required size. The "pomegranate-like" particle represents the collection of nano- and ultra-fine TiB_2 particulates "gluing" together by silicon, as in Figure 2c. This kind of structure may positively contribute to the process of melting/solidification. During laser heating, the ceramic phase TiB_2, which is tightly embedded in Si without formation of the chemical bonds, attains affinity to viscous silicon, thus promoting the sintering and compaction process. Figure 2d displays the XRD pattern of the powder revealing the presence of hexagonal titanium diboride (PDF#65-1073) and no spurious phase formation.

The as-synthesized products of Ti+2B+2Si, corresponding to a composition of 56 wt.%TiB_2–44 wt.%Si, were grinded and sieved to the powder fractions of 90 μm, 45 μm, and 20 μm particle size. Particle size distribution (PSD) and shape factor influence flowability; moreover, the quality of the final product is affected by the thickness and uniformity of each powder layer in the build box [26]. The PSD and flowability of the powders are specified in Table 3. The flowability of the powders with a particle size less than 20 μm was negligible, and no meaningful result was recorded. The powders with a particle size in the range of 20–45 μm demonstrated moderate flowability, which nevertheless was acceptable for the SLM processing to ensure a homogenous and non-porous microstructure.

Table 3. Particle size distribution (PSD) and Hall flow rate of TiB_2-Si powders.

Powder Size, μm	PSD, μm	Hall Flow Rate (FR_H), s/50 g
μ < 20	-	-
20 < μ< 45	Dv10 – 5.48 Dv50 – 21.2 Dv90 – 41.4	29.75 ± 0.31
45 < μ < 90	Dv10 – 12.3 Dv50 – 57.56 Dv90 – 85.4	24.68 ± 0.34

3.2. *Selective Laser Melting*

The structures designed by CAD were adjusted to optimize the SLM procedure in terms of a laser current (I, mA).

The X-ray diffraction pattern of the SLM-ed sample reveals no new or spurious phase formation during the SLM process (Figure 3). The XRD patterns of the SHS powder indicate the presence of 44.1 %Si, while after the SLM process, the amount of Si is calculated to be 43.5%. The difference might be attributed to the accuracy of the Rietveld refinement method; moreover, some evaporation of silicon during the SLM process cannot be avoided at 10–20 mbar pressure. Comparative analysis of the XRD patterns of the powders and printed parts revealed no changes of peak shapes.

The geometric density of the TiB_2-Si compacts printed at the laser current ranging from 1400 to 2200 mA is specified in Table 4. Taking into consideration the theoretical density of the 56 wt.%TiB_2– 44 wt.%Si composite (3.19 g·cm^{-3}), the density of the bulks varies from 2.77 to 3.05 g·cm^{-3} corresponding to a relative density range from ~87 to ~97%. Therefore, a laser current of a high intensity (at least I = 2200 mA) is needed for the production of a high-density material. Cylinder 3, printed at a high energy input, exhibits the highest density due to larger/deeper melt pools, which provides sufficient stitching, melt track overlapping, and improved interlayer connection, resulting in the elimination of the defects caused by lack of fusion. Rapid infiltration of liquid Si into the pores implies readiness of Si to wet TiB_2, assuming a low contact angle resulting in the restricted removal of TiB_2 solid inclusions from silicon [17]. With an increase in a laser current, the viscosity of liquid silicon decreases, and the flattened silicon inclusions homogeneously occupy the distance between the titanium diboride particles being promoted by the "pomegranate-like" morphology of the feedstock.

Due to the "pomegranate-like" structure of the initial powder particles, during the process of cooling, ultra-fine grained TiB_2 particles serve as nucleation centers making the solidification of molten silicon more homogeneous. This prevents the coarsening of silicon grains and decreases the chance of cracking during shrinkage.

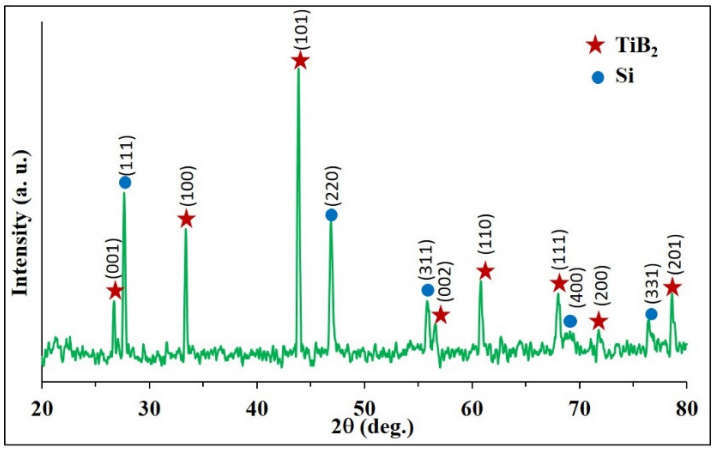

Figure 3. XRD pattern of TiB_2-Si composite after selective laser melting (SLM) (I = 1400 mA).

Table 4. Density and hardness results of TiB_2-Si solid parts.

No.	Geom. Density ($g \cdot cm^{-3}$)	Relative Density (%)	Vickers Hardness (GPa)
Cylinder 1	2.77	87	-
Cylinder 2	2.86	90	4.4 ± 1
Cylinder 3	3.05	97	7.6 ± 1

The microstructures of the composites processed at different laser currents are shown in Figures 4 and 5, which demonstrate some reduction in porosity level with increase in the laser current.

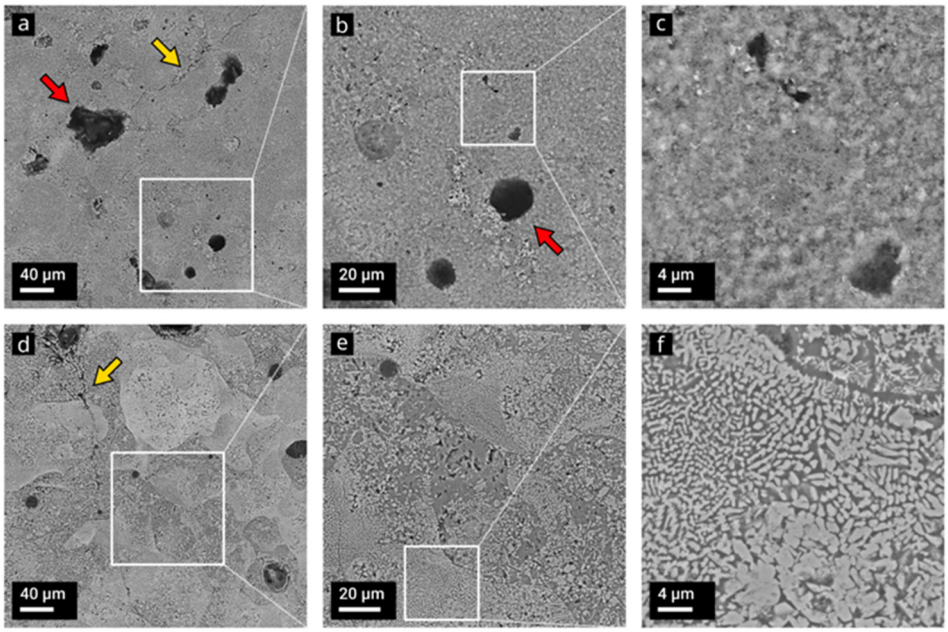

Figure 4. Top surface backscattered electron (BSE) images of TiB_2-Si bulks printed by SLM at 1400 mA (**a**–**c**, Cylinder 1) and 1800 mA laser current (**d**–**f**, Cylinder 2). Cracks and pores are pointed out by yellow and red arrows, respectively.

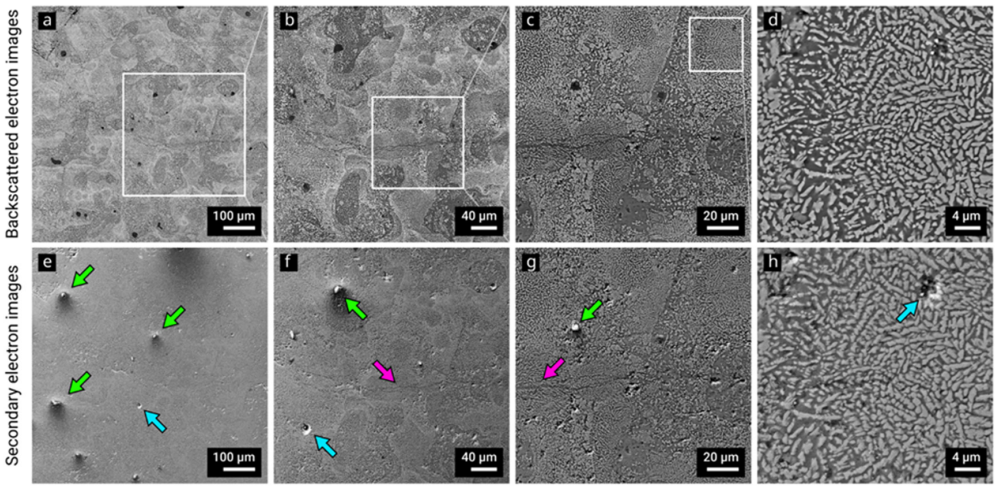

Figure 5. Top surface backscattered electron (**a**–**d**) and secondary electron (SE) images (**e**–**h**) of TiB_2-Si bulks printed by SLM at 2200 mA laser current. Unmelted or partially melted particles are pointed out by green arrows; pores and surface defects are pointed out by blue and pink arrows, respectively.

Process induced non-spherical (irregular shaped) porosity was substantiated by an insufficient energy density (or unexpected disturbances during the printing process) that is needed for complete melting of the feedstock and for promoting consolidation (Figure 4a). If insufficient power is supplied, a lack of fusion regions is identifiable by un-melted powder particles visible near the pores. During the powder bed fusion process, the powder layer and some amount of the underlying substrate undergoes melting; however, an insufficient energy input can result in a decrease in molten pool dimensions and, therefore, in the deficient melting of powder particles and/or re-melting of previously solidified layers.

With the application of a high-power laser, the powder absorbs higher energy as compared to a solidified layer; hence, the temperature of the molten pool increases above the boiling point leading to the vaporization of silicon and possible formation of a plasma state during the SLM process. This immoderate vaporization of silicon melt causes a different kind of defect in the microstructure of the as-built part due to the interplay between the thermo-capillary force introduced by the temperature gradient, drag force induced by the melt flow, and recoil pressure due to material vaporization. The excessive heat input results in enhanced Marangoni flow and the probability of dragging gaseous species (formed by the turbulence of the molten pool or transferred from the as-synthesized TiB_2-Si) into the molten mass. The pressure applied by the silicon vapors leads to the development of spherical pores, which are well-recognized in Figure 4.

At a higher laser current (1800 mA), the specimens with a smoother surface and a higher density can be produced; however, the surface cracks are found in both samples, as seen in Figure 4d–f. In the system under discussion, the fusion defects were observed in the samples produced at 1400–1800 mA laser current, while the spherical pores are identifiable in all bulks caused by the absorbed gas release or by evaporation of the melt.

Hot-tearing porosity is related to the shrinkage during solidification. Upon cooling through the mushy zone, there is an insufficient amount of material to fill the voids in the solidifying material (Figure 4a–d). No clearly recognizable large cracks were observed in the probed region of the sample produced at 2200 mA laser current. The overall microstructure mostly consists of the columnar dendritic grains (Figure 5d,h) with an average spacing in the submicron range, which is formed along the deposited direction due to the high thermal gradients of around 10^3–10^8 K·s^{-1} [27].

An influence of the residual porosity onto the hardness is a well-established phenomenon. Expectedly, the hardness of Cylinder 2 is lower as compared to Cylinder 3. For the sample produced at the lowest laser current (1400 mA), no reliable hardness values were measured due to a high porosity.

The microstructures of the 56 wt.%TiB_2–44 wt.%Si composites are comprised of relatively large columnar grains with 2–10 microns length and hundreds of sub-microns of rather equiaxed grains of

TiB_2 distributed in the silicon matrix. On the SE images of Cylinder 3, the unmelted or partially melted particles (marked with green arrows in Figure 5) trapped on the surface of the sample are clearly recognizable. The relatively large grooves (marked with blue arrows) are generated by material chips removal from the surface, and a few surface defects (marked with pink arrows) are either scratches essentially produced during polishing or segregated silicon in a solidified melt pool; however, further detailed analysis is required to prove or disapprove this statement.

EDS mapping of 3D printed solid parts is shown in Figure 6. Figure 6b–e demonstrates the prevailing presence of Si and a minor concentration of Ti atoms (possible formation of TiSi or Ti_5Si_3 is not detectable by XRD) between TiB_2 grains. The images indicate Ti and B atoms mostly located at the TiB_2 sites.

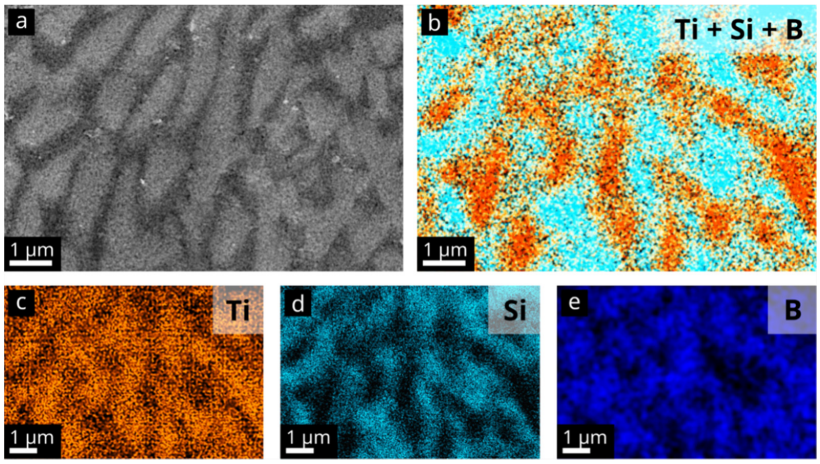

Figure 6. SEM and EDS mapping analysis of selective laser melted TiB_2-Si Cylinder 3 (2200 mA laser current): (**a**) SEM morphology, and (**b**–**e**) is the TiB_2-Si-B map (TiB_2 is marked by orange, Si by blue, top view).

The evaluation of side surface profiles (500 µm × 700 µm) and surface roughness has indicated that both Sa and Sz values are prone to gradually decrease with an increase in the applied laser power, as seen in Figure 7. Cylinder 3 prepared at a laser current of 2200 mA demonstrates the lowest Sa (11.92 µm) and Sz (117.69 µm) for the side surface, i.e., the outer boundary is properly sintered and comprises insignificant surface irregularities.

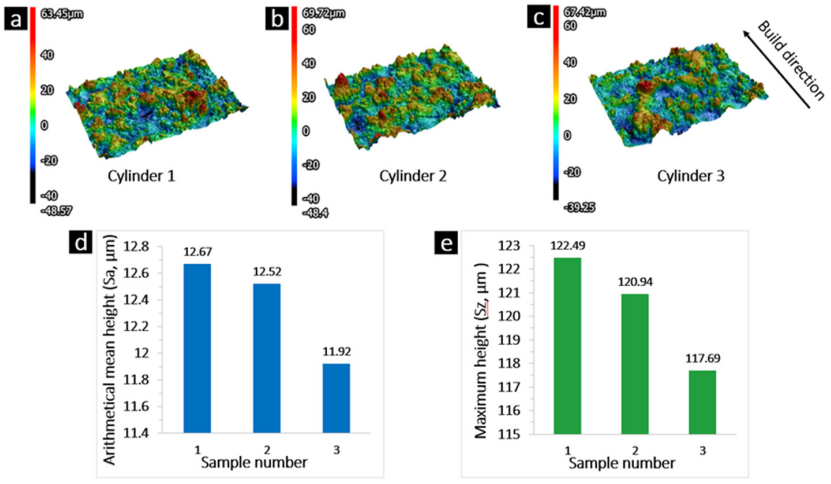

Figure 7. Surface profiles of Cylinders 1, 2, and 3 (**a**–**c**). Average arithmetical mean height (Sa) (**d**), and average maximum height (Sz), (**e**) for Cylinders 1, 2, and 3.

4. Conclusions

For the first time, the "pomegranate-like" structured TiB_2-Si ceramic-metalloid powder feedstock suitable for AM process was prepared by combustion synthesis at a moderate combustion temperature of 1530 °C. As for SHS process, an effective activation energy in the Ti-B-Si system for the slow step was estimated to be 184 kJ. The powder particulates consist of huge amount of nano-scaled TiB_2 particles glued together by silicon. No spurious phases were detected assuming no phase transformation or reaction between the constituents during processing. The powders consisting particles in the range of 20–45 μm demonstrated flowability that may be considered to be acceptable for AM through SLM without any post-treatment/atomization.

The "pomegranate-like" powders demonstrated a high efficiency for manufacturing solid bulks. The 56 wt.%TiB_2–44 wt.%Si composites with a relative density of around 97% and hardness of 6.7 ± 1 GPa (HV1) were processed employing a laser current of 2200 mA and a scanning speed of 80 mm s^{-1}.

Supplementary Materials: The following are available online at http://www.mdpi.com/2076-3417/10/9/3283/s1, Figure S1: Arrhenius plot for the effective activation energy of the Ti-B-Si combustion reaction.

Author Contributions: Conceptualization – I.H. and S.A.; methodology, S.A. and L.L; software, L.L.; validation, I.H., S.A., T.M., and L.L.; formal analysis, I.H., T.M., S.A.; investigation, S.A., T.M., and L.L.; resources, I.H. and S.A.; data curation, I.H. and S.A.; writing—original draft preparation, T.M., and L.L.; writing—review and editing, I.H. and S.A.; supervision, I.H. and S.A.; project administration, I.H.; funding acquisition, I.H. and S.A. All authors have read and agreed to the published version of the manuscript.

Funding: This research was funded by the Estonian Research Council, grants number PSG220 and PRG643, and M-ERA.Net project "HOTselflub" N.20097582-CA.

Acknowledgments: This work was supported by the Estonian Research Council grants (PSG220, S. Aydinyan; and PRG643, I. Hussainova) and M-ERA.Net project "HOTselflub". The authors highly appreciate the European Regional Fund, project number 2014-2020.4.01.16-0183 (Smart Industry Centre), and M. Hussainov from Department of Civil Engineering and Architecture, TalTech, for powder analysis).

Conflicts of Interest: The authors declare no conflict of interest. The funders had no role in the design of the study; in the collection, analyses, or interpretation of data; in the writing of the manuscript, or in the decision to publish the results.

References

1. Rayna, T.; Striukova, L. From rapid prototyping to home fabrication: How 3D printing is changing business model innovation. *Technol. Forecast. Soc. Chang.* **2016**, *102*, 214–224. [CrossRef]
2. Kietzmann, J.; Pitt, L.; Berthon, P. Disruptions, decisions, and destinations: Enter the age of 3D printing and additive manufacturing. *Bus. Horiz.* **2015**, *58*, 209–215. [CrossRef]
3. Yap, C.Y.; Chua, C.K.; Dong, Z.L.; Liu, Z.H.; Zhang, D.Q.; Loh, L.E.; Sing, S.L. Review of selective laser melting: Materials and applications. *Appl. Phys. Rev.* **2015**, *2*, 041101. [CrossRef]
4. Gao, W.; Zhang, Y.; Ramanujan, D.; Ramani, K.; Chen, Y.; Williams, C.B.; Wang, C.C.; Shin, Y.C.; Zhang, S.; Zavattieri, P.D. The status, challenges, and future of additive manufacturing in engineering. *Comput. Aided Design.* **2015**, *69*, 65–89. [CrossRef]
5. Sing, S.L.; Yeong, W.Y.; Wiria, F.E.; Tay, B.Y.; Zhao, Z.; Zhao, L.; Tian, Z.; Yang, S. Direct selective laser sintering and melting of ceramics: A review. *Rapid Prototyp. J.* **2017**, *23*, 611–623. [CrossRef]
6. Bourell, D.; Kruth, J.P.; Leu, M.; Levy, G.; Rosen, D.; Beese, A.M.; Clare, A. Materials for additive manufacturing. *CIRP Ann.* **2017**, *66*, 659–681. [CrossRef]
7. Travitzky, N.; Bonet, A.; Dermeik, B.; Fey, T.; Demut, I.F.; Schlier, L.; Schlordt, T.; Greil, P. Additive Manufacturing of Ceramic-Based Materials. *Adv. Eng. Mater.* **2014**, *16*, 729–754. [CrossRef]
8. DebRoy, T.; Wei, H.L.; Zuback, J.S.; Mukherjee, T.; Elmer, J.W.; Milewski, J.O.; Beese, A.M.; Wilson-Heid, A.; Ded, A.; Zhang, W. Additive manufacturing of metallic components–Process, structure and properties. *Prog. Mater. Sci.* **2018**, *92*, 112–224. [CrossRef]
9. Minasyan, T.; Aghayan, M.; Aydinyan, S.; Liu, L.; Hussainova, I. Combustion synthesis of MoSi2 based composite and selective laser sintering thereof. *J. Eur. Ceram. Soc.* **2018**, *38*, 3814–3821. [CrossRef]

10. Varma, A.; Rogachev, A.S.; Mukasyan, A.S.; Hwang, S. Combustion synthesis of advanced materials: Principles and applications. In *Advances in Chemical Engineering*; Academic Press: Cambridge, MA, USA, 1998; Volume 24, pp. 79–226. [CrossRef]
11. Bogdanov, S.P.; Sychov, M.M.; Lebedev, L.A.; Mjakin, S.V.; Gravit, M.V. Core-shell powders for additive manufacturing of articles for underground construction. *Procedia Eng.* **2016**, *165*, 1579–1586. [CrossRef]
12. Minasyan, T.; Liu, L.; Holovenko, Y.; Aydinyan, S.; Hussainova, I. Additively manufactured mesostructured $MoSi_2$-Si_3N_4 ceramic lattice. *Ceram. Int.* **2019**, *45*, 9926–9933. [CrossRef]
13. Telle, R. Analysis of pressureless sintering of titanium diboride ceramics with nickel, cobalt, and tungsten carbide additives. *J. Eur. Ceram. Soc.* **2019**, *39*, 2266–2276. [CrossRef]
14. Basu, B.; Raju, G.B.; Suri, A.K. Processing and properties of monolithic TiB_2 based materials. *Int. Mater. Rev.* **2006**, *51*, 352–374. [CrossRef]
15. Liu, L.; Aydinyan, S.; Minasyan, T.; Baronins, J.; Antonov, M.; Kharatyan, S.; Hussainova, I. Spark plasma sintering of combustion synthesized TiB_2-Si composite. *Ceram. Mod. Technol.* **2019**, *1*. [CrossRef]
16. Bertrand, P.; Bayle, F.; Combe, C.; Gœuriot, P.; Smurov, I. Ceramic components manufacturing by selective laser sintering. *Appl. Surf. Sci.* **2007**, *254*, 989–992. [CrossRef]
17. Li, X.P.; Ji, G.; Chen, Z.; Addad, A.; Wu, Y.; Wang, H.W.; Vleugels, J.; van Humbeeck, J.; Kruth, J.P. Selective laser melting of nano-TiB2 decorated AlSi10Mg alloy with high fracture strength and ductility. *Acta Mater.* **2017**, *129*, 183–193. [CrossRef]
18. Attar, H.; Bönisch, M.; Calin, M.; Zhang, L.C.; Scudino, S.; Eckert, J. Selective laser melting of in situ titanium–titanium boride composites: Processing, microstructure and mechanical properties. *Acta Mater.* **2014**, *76*, 13–22. [CrossRef]
19. Shishkovsky, I.; Kakovkina, N.; Sherbakov, V. Graded layered titanium composite structures with TiB_2 inclusions fabricated by selective laser melting. *Compos. Struct.* **2017**, *169*, 90–96. [CrossRef]
20. Xia, M.; Liu, A.; Hou, Z.; Li, N.; Chen, Z.; Ding, H. Microstructure growth behavior and its evolution mechanism during laser additive manufacture of in-situ reinforced (TiB+TiC)/Ti composite. *J. Alloy. Compd.* **2017**, *728*, 436–444. [CrossRef]
21. Lee, H.; Lim, C.H.J.; Low, M.J.; Tham, N.; Murukeshan, V.M.; Kim, Y.J. Lasers in additive manufacturing: A review. *Int. J. Precis. Eng. Manuf. Green Technol.* **2017**, *4*, 307–322. [CrossRef]
22. Sani, E.; Meucci, M.; Mercatelli, L.; Jafrancesco, D.; Sans, J.L.; Silvestroni, L.; Sciti, D. Optical properties of boride ultrahigh-temperature ceramics for solar thermal absorbers. *J. Photonics Energy* **2014**, *4*, 045599. [CrossRef]
23. Riley, D.P.; Oliver, C.P.; Kisi, E.H. In-situ neutron diffraction of titanium silicide, Ti5Si3, during self-propagating high-temperature synthesis (SHS). *Intermetallics* **2006**, *14*, 33–38. [CrossRef]
24. Li, H.P. The numerical simulation of the heterogeneous composition effect on the combustion synthesis of TiB_2 compound. *Acta Mater.* **2003**, *51*, 3213–3224. [CrossRef]
25. Li, H.P. A numerical investigation of the ignition power on micropyretic synthesis of TiB_2. *Model. Simul. Mater. Sci. Eng.* **2005**, *13*, 1331. [CrossRef]
26. Kennedy, S.K.; Dalley, A.M.; Kotyk, G.J. Additive Manufacturing: Assessing Metal Powder Quality through Characterizing Feedstock and Contaminants. *J. Mater. Eng. Perform.* **2019**, *28*, 728–740. [CrossRef]
27. Gu, D.D.; Meiners, W.; Wissenbach, K.; Poprawe, R. Laser additive manufacturing of metallic components: Materials, processes and mechanisms. *Inter. Mater. Rev.* **2012**, *57*, 133–164. [CrossRef]